AGU PUBLICATIONS

Geophysical Research Letters

RESEARCH LETTER
10.1002/2017GL072819

K.A. McColl and W. Wang contributed equally.

Key Points:
- Soil moisture drydowns encode information on loss terms in the water budget
- We estimate drydown time scales globally using one year of SMAP observations
- The time scale decreases with increasing aridity and soil sand content

Supporting Information:
- Supporting Information S1

Correspondence to:
H. Lu,
luhui@tsinghua.edu.cn

Citation:
McColl, K. A., W. Wang, B. Peng, R. Akbar, D. J. Short Gianotti, H. Lu, M. Pan, and D. Entekhabi (2017), Global characterization of surface soil moisture drydowns, *Geophys. Res. Lett.*, *44*, doi:10.1002/2017GL072819.

Received 25 JAN 2017
Accepted 10 APR 2017
Accepted article online 18 APR 2017

Global characterization of surface soil moisture drydowns

Kaighin A. McColl[1], Wei Wang[2], Bin Peng[3], Ruzbeh Akbar[4], Daniel J. Short Gianotti[4], Hui Lu[2,5], Ming Pan[6], and Dara Entekhabi[4]

[1]Department of Earth and Planetary Sciences, Harvard University, Cambridge, Massachusetts, USA, [2]Ministry of Education Key Laboratory for Earth System Modeling, Department of Earth System Science, Tsinghua University, Beijing, China, [3]National Center for Supercomputing Applications and Department of Natural Resources and Environmental Sciences, University of Illinois at Urbana-Champaign, Urbana, Illinois, USA, [4]Department of Civil and Environmental Engineering, Massachusetts Institute of Technology, Cambridge, Massachusetts, USA, [5]Joint Center for Global Change Studies, Beijing, China, [6]Department of Civil and Environmental Engineering, Princeton University, Princeton, New Jersey, USA

Abstract Loss terms in the land water budget (including drainage, runoff, and evapotranspiration) are encoded in the shape of soil moisture "drydowns": the soil moisture time series directly following a precipitation event, during which the infiltration input is zero. The rate at which drydowns occur—here characterized by the exponential decay time scale τ—is directly related to the shape of the loss function and is a key characteristic of global weather and climate models. In this study, we use 1 year of surface soil moisture observations from NASA's Soil Moisture Active Passive mission to characterize τ globally. Consistent with physical reasoning, the observations show that τ is lower in regions with sandier soils, and in regions that are more arid. To our knowledge, these are the first global estimates of τ—based on observations alone—at scales relevant to weather and climate models.

1. Introduction

Soil moisture plays an important role in hydrological processes fundamental to agriculture [e.g., *Rosenzweig et al.*, 2002; *Botter et al.*, 2007], ecosystem function [e.g., *D'Odorico et al.*, 2003; *Manzoni et al.*, 2012], and human health [e.g., *Fecan et al.*, 1999; *Bomblies and Eltahir*, 2010]. It regulates exchanges of water, heat, and other scalars between the land and atmosphere [*Brutsaert*, 1982] and impacts the development and persistence of droughts, floods, and heat waves [e.g., *Entekhabi et al.*, 1996; *Bonan and Stillwell-Soller*, 1998; *Lorenz et al.*, 2010]. In a planar homogeneous soil volume, its dynamics are governed by the vertically integrated water budget:

$$\Delta z \frac{\mathrm{d}\theta}{\mathrm{d}t} = P(t) - L(\theta, t) = P(t) - (D(\theta, t) + ET(\theta, t) + Q(\theta, t)), \tag{1}$$

where θ is volumetric soil moisture (–), t is time (T), Δz is the depth of the soil volume below the surface (L), $P(t)$ is the precipitation rate (L T^{-1}), and $L(t)$ is the rate at which water is lost from the volume due to runoff ($Q(\theta, t)$), drainage ($D(\theta, t)$), and evapotranspiration ($ET(\theta, t)$) (L T^{-1}). It is natural to combine these fluxes into the single function L since they are quasi-deterministic characteristics of the land surface [*Delworth and Manabe*, 1988; *Ghannam et al.*, 2016], compared to precipitation, which is an exogenous forcing and often modeled stochastically.

Various forms of the loss function $L(\theta)$ have been proposed in the literature [*Rodriguez-Iturbe et al.*, 1999a; *Laio et al.*, 2001a]. These loss functions typically include three regimes (Figure 1a). First, for wet soils ($\theta > \theta_{fc}$), drainage and runoff dominate. To first order, L follows a power law, increasing with increasing soil moisture. Second, for intermediate wetness ($\theta_* < \theta \leq \theta_{fc}$), the drainage flux reduces and L is dominated by evapotranspiration, which is purely a function of atmospheric demand and therefore invariant with respect to soil moisture. This phase is termed "stage I" evapotranspiration. Third, for drier soils ($\theta_w < \theta \leq \theta_*$), evapotranspiration becomes limited by soil water availability, and L declines to zero as soil moisture decreases. This phase is termed "stage II" evapotranspiration. The stage I ET and stage II ET losses are often modeled as

$$L(\theta) = \begin{cases} E_{max}, \text{ if } \theta_* < \theta \leq \theta_{fc} \\ \beta(\theta) E_{max}, \text{ if } \theta_w < \theta \leq \theta_*, \end{cases} \tag{2}$$

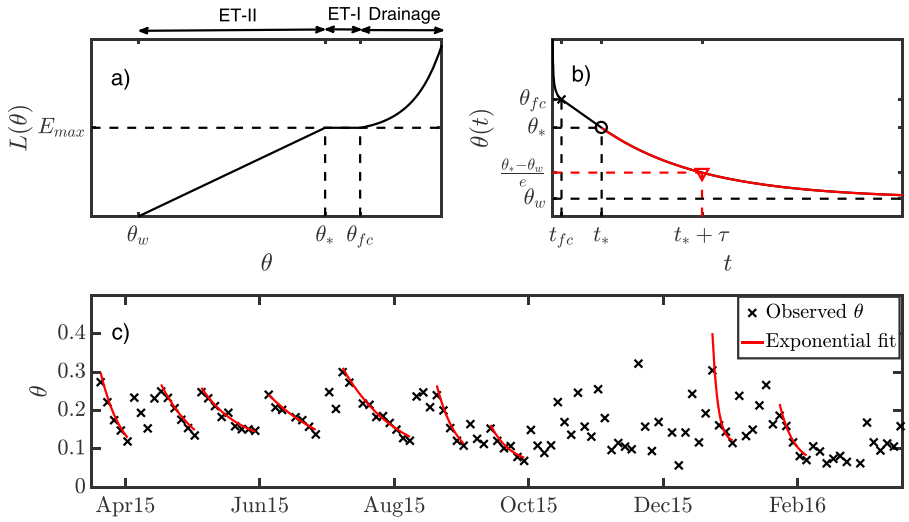

Figure 1. (a) Example soil moisture (θ) loss function $L(\theta)$ based on the model of *Laio et al.* [2001a]. The model has three different regimes: drainage dominated ($\theta > \theta_{fc}$), stage I ET (ET-I, $\theta_* < \theta \leq \theta_{fc}$), and stage II ET (ET-II, $\theta_w < \theta \leq \theta_*$), where θ_{fc} is the field capacity, θ_* is a transitional soil moisture, θ_w is the wilting point, and E_{max} is the maximum possible *ET*, given constraints of weather and plant physiology. (b) Example soil moisture drydown time series (black line) following a rainfall pulse, based on the model of *Laio et al.* [2001a]. The transition from drainage dominated to stage I ET occurs at time t_{fc} (black cross); the transition from stage I ET to stage II ET occurs at time t_* (black circle). The drydown time series is typically dominated by stage II ET (red line), characterized by the *e*-folding time τ (red triangle). (c) One year of SMAP soil moisture observations (black crosses) for a site near Brisbane, Australia. The red lines show the exponential model fits to the drydowns identified by the algorithm used in this study. Equivalent plots for sites in Eastern Europe, Africa, central Asia, USA, Brazil, and Saudi Arabia are presented in the supporting information (Figures S1–S6).

where E_{max} ($L\,T^{-1}$) is the maximum potential evapotranspiration and $\beta(\theta) = \frac{\theta(t)-\theta_w}{\theta_*-\theta_w}$ (–) [*Manabe*, 1969; *Jacquemin and Noilhan*, 1990; *Mahfouf et al.*, 1996; *Rodriguez-Iturbe et al.*, 1999b]. The loss function has also been estimated directly from collocated observations of precipitation and soil moisture using a technique that exploits the stationarity of the soil moisture time series [*Salvucci*, 2001]. The loss functions estimated using this method agree qualitatively with the functional form proposed in earlier studies, both at the point scale [*Salvucci*, 2001; *Saleem and Salvucci*, 2002] and at the scale of spaceborne observations [*Tuttle and Salvucci*, 2014]. While many previous studies estimated the loss function for root-zone soil moisture (RZSM, ~1 m depth), and the loss function model in Figure 1a was originally designed for and applied to RZSM, the focus of this study is on surface soil moisture (SSM, 5 cm depth). Based on *Tuttle and Salvucci* [2014], who estimated the SSM loss function over the United States using satellite soil moisture observations, the form given in Figure 1a appears reasonable for the SSM storage.

The loss function is encoded in soil moisture "drydowns": the time series of soil moisture immediately following infiltration of precipitation into the soil, for which $P(t) = 0$ (Figure 1b). In many cases, the drainage and stage I evapotranspiration phases occur rapidly, and the drydown is dominated by stage II evapotranspiration. It is modeled by assuming that all other fluxes are negligible and that *ET* is linearly related to available soil water such that

$$\frac{d\theta}{dt} = -\frac{ET(\theta,t)}{\Delta z} = -\frac{\theta(t)-\theta_w}{\tau} = -\beta(\theta)\frac{E_{max}}{\Delta z}. \tag{3}$$

This model has two parameters: the *e*-folding time scale $\tau = \frac{\Delta z(\theta_*-\theta_w)}{E_{max}}$ (*T*) and θ_w (–). Global estimates of these parameters are essential inputs to climate models [*Sellers et al.*, 1997]. For models with different *ET* parameterizations, τ remains an important validation statistic. The parameter τ is of particular interest as a measure of the "memory" of both the RZSM storage [*Koster and Suarez*, 2001; *Seneviratne et al.*, 2006; *Katul et al.*, 2007; *Orth and Seneviratne*, 2012] and the SSM storage [*McColl et al.*, 2017]. Sufficient soil moisture memory is a necessary condition for the occurrence of soil moisture-precipitation feedbacks [*Koster and Suarez*, 2003].

Values of τ vary considerably between models [*Mahfouf et al.*, 1996; *Teuling et al.*, 2006], and between limited observations at individual sites [*Kurc and Small*, 2004; *Dardanelli et al.*, 2004; *Williams and Albertson*, 2004;

Teuling et al., 2006; *Brutsaert*, 2014], typically varying between several and ~20 days. Global estimates at the large scales required for climate models are typically obtained by upscaling point estimates using uncertain land cover or vegetation maps. The accuracy of these estimates at climate model grid scales is unclear.

Global observations of SSM at scales relevant to weather and climate models are now available from spaceborne observations, such as the European Space Agency's Soil Moisture Ocean Salinity (SMOS) mission [*Kerr et al.*, 2010], and the National Aeronautics and Space Administration's Soil Moisture Active Passive (SMAP) mission [*Entekhabi et al.*, 2010]. SSM — defined in this study as the vertically integrated soil moisture of the top 5 cm soil layer — may become decoupled from RZSM in arid environments. However, while RZSM can have a stronger relation to hydrological fluxes such as *ET*, SSM is often well correlated with RZSM [*Ford et al.*, 2014]. In this study, we use 1 year of global SSM observations from SMAP to characterize τ globally. Preliminary comparisons between SMAP and in situ SSM observations suggest SMAP is meeting its performance target, after accounting for differences between the lateral and vertical support of satellite and in situ soil moisture observations [*Chan et al.*, 2016; *Shellito et al.*, 2016]. In section 2, we describe the SMAP observations and other data used in this study. We also describe the algorithm used to identify soil moisture drydowns, and the procedure for estimating τ. In section 3, we present and discuss the results of the analysis, including global maps of average values of τ, and characterize its dependence on soil properties and climate.

2. Methods

In this section, we describe the data used in the analysis and the procedure for estimating drydown parameters from SSM observations.

2.1. SMAP Soil Moisture Data

The NASA SMAP satellite was launched in January 2015 and measures soil moisture globally every 2–3 days [*Entekhabi et al.*, 2010]. SMAP originally included an L band radar and radiometer, providing 3 km and 36 km soil moisture observations, respectively. The radar ceased operations after 11 weeks due to an instrument anomaly; however, the radiometer continues to provide global soil moisture observations, which are used in this study [*O'Neill et al.*, 2016]. We use observations spanning the first full annual cycle of SMAP observations: 1 April 2015 to 31 March 2016. Retrievals impacted by radio frequency interference, the presence of water bodies (>5% coverage of a pixel), dense vegetation cover (> 5 kg/m^2), frozen soil, ice, or snow (surface temperatures below 0°C) were removed from the analysis. In northern latitudes, data from a substantial portion of the year are discarded due to frozen soil. While this biases the sampling of drydown events to mainly spring and summer months in these regions, drydown events cannot occur while the soil is frozen; therefore, the biased sampling is not expected to affect our conclusions.

The estimated parameters in this study — in particular, the drydown time scales τ — are nontrivially dependent on the sampling frequency of the soil moisture observations. For example, given a monthly time series ($f \approx 1/30$ day^{-1}) of soil moisture observations, it is clearly impossible to identify rapid drydowns where, e.g., $\tau \sim 1$ day. Furthermore, while the SMAP sampling frequency is nominally $f = 1/3$ day^{-1}, the effective sampling frequency — the ratio of the total number of soil moisture observations available at a given location to the total number of days in the study period — deviates from this value in many locations due to the geometry of SMAP's polar orbit and the locations of overlapping swaths. The effective sampling frequency can also be reduced by filtering of observations to exclude erroneous retrievals in regions with, for example, dense vegetation, water bodies, or frozen soil. The resulting global map of the SMAP effective sampling frequency includes coherent spatial patterns that can result in spatially coherent patterns in maps of drydown parameters that are solely due to differences in sampling frequency, rather than differences in physical processes controlling drydowns. Therefore, to mitigate this bias, we thinned the SMAP observations in regions where $f > \frac{1}{3}$ day^{-1} to obtain an effective sampling frequency of $f \approx \frac{1}{3}$ day^{-1} in these regions (supporting information Figure S9). This mitigates the impacts of spatial differences in sampling frequency on our analysis. Since the effective sampling frequency differs subtly between different satellite soil moisture products, we do not use soil moisture observations from other soil moisture satellite missions — such as SMOS — in this study.

2.2. Ancillary Data

Soil texture data are obtained from composites prepared for the SMAP mission [*Das*, 2013].

Land cover classifications from the Moderate Resolution Imaging Spectroradiometer (MODIS) MCD12Q1 International Geosphere and Biosphere Programme (IGBP) collection 5 land cover product are used [*Friedl et al.*, 2010]. No SMAP soil moisture observations are available in regions classified as "evergreen broadleaf forest,"

"wetlands," "urban," or "frozen" due to filtering detailed in the previous section. These land cover classes are therefore not represented in the analyses below.

Fields from the Noah 2.7.1 model in the Global Land Data Assimilation System (GLDAS) [*Rodell and Beaudoing*, 2007] are used to estimate an aridity index. Specifically, the aridity index is defined as $A = \frac{R_n}{\lambda P}$, where λ is the latent heat of vaporization (J kg^{-1}), R_n is the mean daily net radiation (W m^{-2}), and P is the mean daily precipitation (kg m^{-2}). This index is a measure of aridity that is independent of the SMAP soil moisture observations. Higher values indicate greater aridity.

2.3. Identification of Drydowns

Drydowns were identified in the soil moisture time series as periods in which the temporal change in soil moisture was consistently negative. By introducing a positive temporal increment into a series of negative increments, noise in the observations has the potential to truncate real drydowns and to create spurious ones. To avoid noise truncating real drydowns, any positive increment smaller than 5% of the observed range of soil moisture at the site is excluded if it would otherwise truncate a drydown. To avoid noise creating spurious drydowns, identified drydowns were excluded from the analysis when the positive increment preceding the drydown was less than two times the target unbiased root-mean-square difference for SMAP observations (0.08). Of the remaining drydowns, only those that contained more than three SMAP observations were retained.

For each drydown period, an exponential model [*Rondinelli et al.*, 2015; *Shellito et al.*, 2016] of the form

$$\theta(t) = \Delta\theta \exp\left(-\frac{t}{\hat{\tau}}\right) + \hat{\theta}_w \tag{4}$$

was fit to each drydown that consisted of at least four SMAP observations, using nonlinear least squares fitting. Here $\theta(t)$ is the volumetric soil moisture content (–) observed t days after the start of the drydown, $\Delta\theta$ is the positive increment in soil moisture (–) that precedes the drydown, $\hat{\tau}$ is the estimated drydown e-folding time scale (days), and $\hat{\theta}_w$ is the estimated lower bound of soil moisture (–), approached asymptotically by the soil moisture time series. Consistent with *Shellito et al.* [2016], we constrain $\hat{\theta}_w$ to be less than the lowest soil moisture observed during the drydown, and greater than or equal to the lowest soil moisture observed over the full time period (an estimate of the residual soil moisture). Therefore, $\hat{\theta}_w$ is an "effective" wilting point that, in practice, is likely smaller than the true wilting point. This distinction has little impact on our estimates of $\hat{\tau}$, which is the main focus of this analysis. We only retained drydowns if the coefficient of determination (R^2) of the exponential fit to the SMAP observations was at least 0.7 (supporting information Figure S8). The median estimated drydown parameters are plotted globally. Median estimated parameters are only plotted in locations where there are at least three observed drydowns. The total number of drydowns identified at a given location globally is shown in supporting information Figure S10.

We distinguish between the estimated quantities ($\hat{\tau}$, $\hat{\theta}_w$) and their true values (τ, θ_w). Our estimates are subject to sampling error, like any statistical estimate. In addition to this error source, by fitting an exponential curve to each SMAP-observed drydown, we expect $\hat{\tau}$ will be identical to τ in cases where the drydown is dominated by stage II ET (i.e., t_* is substantially smaller than the duration of the drydown). In cases where this is not the case—particularly in wet, cold regions with high clay fraction soils—then $\hat{\tau}$ will be typically smaller than τ. Simulations using the model of *Laio et al.* [2001a] applied to a 5 cm soil volume over a broad range of soil types and climate conditions (supporting information Figures S5 and S6 and Text S1) suggest t_* rarely ever exceeds 5 days and is often less than 3 days. The SMAP revisit time is approximately once every 3 days, meaning that for drydowns with $t_* < 3$ days, $\hat{\tau}$ and τ will be identical, on average. In a limited number of cases, where $t_* > 3$ days, there will be some impact on the estimate of $\hat{\tau}$. Even then, only the first one or two SMAP observations in the drydown will deviate from the exponential form. Each drydown consists of at least four SMAP observations, spanning at least 9 days; and in many regions, the median drydown length is considerably longer than this (supporting information Figure S13). Therefore, while $\hat{\tau}$ and τ will differ in some cases, the deviations will likely be small.

Unlike some previous studies, we do not use model precipitation time series to assist in identifying soil moisture drydowns. The aim of this study is to characterize average properties of surface soil moisture drydowns globally using observations alone. We perform several checks to ensure that the identified drydowns are not the result of noise. Furthermore, estimates of average drydown properties—the focus of this study—will not be substantially affected by a limited number of misidentified drydowns.

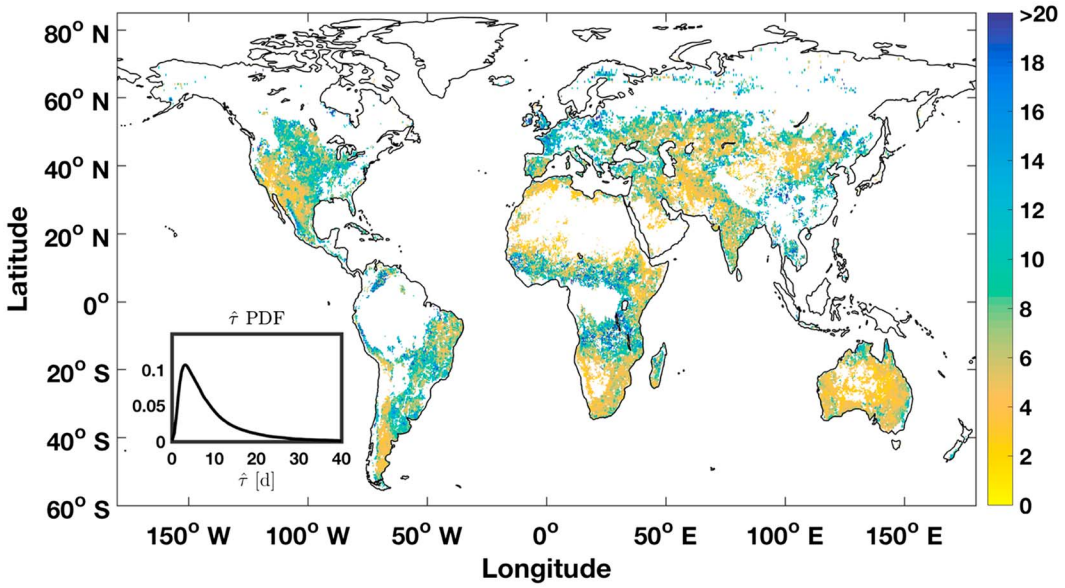

Figure 2. Median drydown time scale $\hat{\tau}$ (day). Inset: estimated probability density function (PDF) of $\hat{\tau}$. White regions were excluded from the analysis due to radio frequency interference, soil freezing, presence of small waterbodies, dense vegetation cover, or if less than three drydown events were identified.

3. Results and Discussion

In this section, we present the results of the analysis, compare the results with recent published studies, and discuss limitations of the analysis.

The key parameter of interest—the estimated median *e*-folding drydown time scale—is mapped globally in Figure 2. Globally, the distribution of $\hat{\tau}$ is highly (positively) skewed, with a mode of $\hat{\tau} = 3$ days, but a heavy tail. The modal value agrees well with estimated values of $\tau = 2.8$ and 2.5 days estimated using in situ soil moisture observations at a grassland and shrubland, respectively [*Kurc and Small*, 2004] and is consistent with SSM dynamics observed during a field campaign in southeastern Australia [*Teuling et al.*, 2007]. While there is considerable heterogeneity in the map of observed median $\hat{\tau}$, coherent patterns are also visible. In the United States, the semiarid western U.S. displays a drydown time scale on the order of a few days (with considerable variability). In the central and eastern U.S., however, the drydown time scale is considerably higher, on the order of 10 days. The global map of $\hat{\theta}_w$ (supporting information Figure S7) displays less heterogeneity, as expected, since it is mostly a function of static soil properties, except in persistently wet climates. Its modal value is 0.02, and its distribution also exhibits considerable density in the right tail. The SMAP algorithm imposes a hard lower bound on soil moisture retrievals, which may contribute to the peak in the probability density function (PDF) around $\hat{\theta}_w = 0.02$. Therefore, it is unclear if the peak in $\hat{\theta}_w$ is physical or a measurement artifact. However, this will have little effect on our estimates of $\hat{\tau}$.

While the drydown time scale is spatially heterogeneous, we examine its relation to three important covariates in Figure 3. Sandy soils have larger pores with lower suction caused by surface tension forces and therefore release water to the atmosphere via evapotranspiration more readily. The results in Figure 3 (top left) are consistent with this, showing that $\hat{\tau}$ systematically decreases with increasing sand fraction, albeit with substantial variability around this relation. We further expect that soils will lose water to the atmosphere more rapidly in more arid environments, where evapotranspiration is only limited by water availability. This is confirmed in Figure 3 (top right), which shows that $\hat{\tau}$ decreases with increasing aridity. There remains substantial unexplained variance in observations of $\hat{\tau}$. Much of this is likely due to vegetation, which is expected to have a significant and spatially heterogeneous impact on τ [*Porporato et al.*, 2001; *Laio et al.*, 2001b; *Teuling et al.*, 2006]. However, there is no clear relation between IGBP land cover classes and $\hat{\tau}$ (Figure 3 (bottom)), and $\hat{\tau}$ varies substantially within most land cover classes. Land cover classifications only crudely characterize the heterogeneous responses of vegetation to water stress [*Konings and Gentine*, 2016], which may explain the unclear relation between land cover type and $\hat{\tau}$. Overall, these results emphasize the importance of

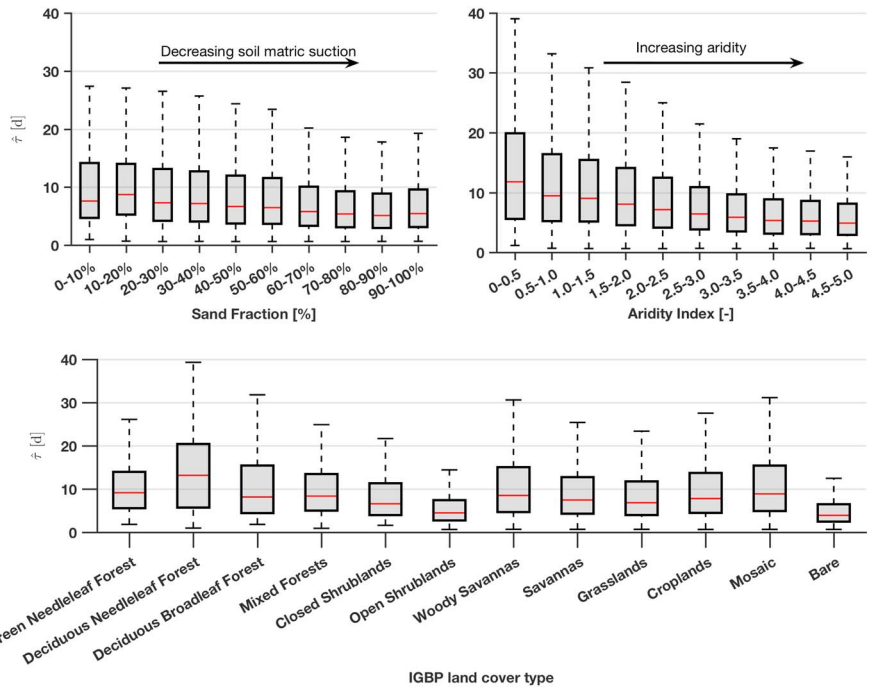

Figure 3. Box plots showing variation of (top left) $\hat{\tau}$ globally with sand fraction (%), (top right) aridity index A (−), and (bottom) IGBP land cover type. Box plots show the median (red horizontal line), 25th and 75th percentiles (top and bottom of the grey shaded box, respectively), and maximum and minimum observed values (edges of the top and bottom whiskers, respectively).

parameterizing τ (or equivalent parameters) in land surface models using observations, rather than relying on relations with covariates such as those considered in Figure 3.

3.1. Comparison With Recent Studies

A recent study [*McColl et al.*, 2017] found that SSM memory is longest in arid regions (low mean soil moisture). This result may appear to be in conflict with Figure 3 (top right). However, the results are readily reconciled by noting that $\hat{\tau}$ is an evaporative time scale that ignores drainage; *McColl et al.* [2017] include drainage in their analysis. Drainage is a substantially more rapid flux and dominates losses compared with ET in wet conditions (Figure 1). Therefore, including its effects in a loss time scale will result in a shorter time scale estimate, particularly in wet regions. In arid regions the drainage flux is small due to low soil moisture; therefore, an estimated loss time scale that includes drainage will likely be longest in arid regions (as found in *McColl et al.* [2017]), explaining the difference with Figure 3 (top right). Therefore, the differences between the results presented here and in *McColl et al.* [2017] are expected due to the exclusion of drainage fluxes in this analysis.

Soil moisture drydowns have attracted interest in the context of validating satellite estimates of soil moisture. Two recent studies found that satellite estimates of soil moisture drydowns are more rapid than those estimated from in situ observations [*Rondinelli et al.*, 2015; *Shellito et al.*, 2016]. Another found varying results, with satellite-estimated soil moisture drydowns sometimes faster, and sometimes slower, than in situ estimates [*Champagne et al.*, 2016]. Preliminary validation studies suggest that SMAP is meeting its performance targets [*Chan et al.*, 2016; *Pan et al.*, 2016]. Therefore, differences between satellite and in situ estimates of soil moisture drying rates are likely due to differences between the vertical and lateral support of satellite and in situ measurements, rather than systematic errors in the satellite retrievals.

3.2. Limitations

Our analysis is subject to several limitations. First, SMAP measures SSM rather than RZSM, and our estimates of $\hat{\tau}$ pertain to SSM rather than RZSM. Since many land surface models do not include an explicit SSM layer, care must be taken in directly comparing τ from land surface models with values estimated in this study. However, since SSM and RZSM are often correlated, the SMAP-estimated values of τ provided in this study may still be of use in parameterizing land surface models, provided differences between SSM and RZSM are taken into consideration.

Second, like any metric of soil moisture memory, our estimates of $\hat{\tau}$ are dependent on the sampling frequency of the observations [*McColl et al.*, 2017]. Drydowns that occur on time scales smaller than the SMAP repeat time (approximately every 2–3 days) will not be resolved by the observations, potentially positively biasing estimates of average $\hat{\tau}$. However, modeling based on decades of field observations at the point scale suggest that only regions with a high sand content and arid conditions are likely to be affected (supporting information Figures S5 and S6 and Text S1). These observations are largely masked out in our analysis already, as they typically do not contain enough drydowns. Another limitation due to finite sampling frequency is the inability to resolve different phases of the drydown (Figure 1). We assume that drainage and stage I ET occur rapidly, and therefore, stage II ET is the dominant process governing the shape of the drydown resolved by the SMAP observations. In some cases, particularly wet regions with low atmospheric evaporative demand and/or a high clay fraction, modeling suggests that it is possible that a drydown may take up to 5 days to reach stage II ET (supporting information Figures S5 and S6 and Text S1). In this case, the early phase of the drydown will be resolved by the SMAP observations but will be linear rather than exponential, resulting in $\hat{\tau} < \tau$. However, very few regions are expected to be impacted by this possible bias, particularly since many regions in northern latitudes are already excluded from this analysis. *Shellito et al.* [2016] estimated $\hat{\tau}$ using hourly ($f = 24$ day^{-1}) in situ surface soil moisture observations at 17 sites. They found that thinning the soil moisture observations to $f = \frac{1}{3}$ day^{-1} had only a small impact on the estimated $\hat{\tau}$ at most sites. Overall, the sampling frequencies of SMAP and other L band soil moisture missions such as SMOS [*Kerr et al.*, 2010] of $f = \frac{1}{3}$ day^{-1} are the highest available at global scales and are capable of resolving a substantial fraction of drydown variability.

Third, the soil moisture observations are impacted by measurement noise. Fluctuations in the soil moisture time series due to noise may result in detection of spurious drydown events. To counter this, our drydown detection algorithm ignores detected drydowns for which the positive increment in soil moisture preceding the drydown is less than a threshold. In some locations, the threshold may be too high and therefore result in the algorithm missing true drydown events. In other locations, it may be too low and result in the algorithm still detecting some spurious drydown events that are solely attributable to noise. However, sensitivity tests (not shown) demonstrate that the results presented in this study are robust to reasonable changes in the choice of threshold.

Fourth, the results in this study are estimated from 1 year of data. This is typically sufficient to characterize, to first-order, average properties of soil moisture, while recognizing that in some regions, the estimated values will differ from their true climatological value. This assertion is supported by the fact that the global map of estimated $\hat{\tau}$ (Figure 2) contains contiguous, spatially coherent regions (e.g., in the western and central United States) that are consistent with physical reasoning.

4. Conclusions

The soil moisture water balance contains both stochastic (infiltration) and quasi-deterministic (losses including drainage, runoff, and ET) fluxes. Analysis of soil moisture drydowns focuses on the quasi-deterministic processes in the water balance and facilitates characterization of the loss function $L(\theta)$. Characterization of $L(\theta)$ at large scales globally is essential for parameterizing global weather and climate models. In this study, we have characterized the crucial drydown time scale $\hat{\tau}$ globally, using the first year of SSM observations from SMAP. The observations show that $\hat{\tau}$ decreases with increasing soil sand content, consistent with the fact that soil suction—and, therefore, the soil's ability to retain water in the presence of ET—also decreases with increasing sand content. The observations also show that $\hat{\tau}$ decreases with increasing aridity, consistent with the fact that the atmospheric demand for water from the soil is more intense in arid climates. For both relations, however, there is substantial unexplained variance that is likely due to vegetation effects, which are not well characterized by IGBP land cover classification. This analysis provides the first observations-based estimates of τ with coverage and resolution suitable for use in global weather and climate models. As the data record grows with time, it will be interesting to examine seasonal variations in $\hat{\tau}$ and to characterize spatial differences in its full distribution, beyond average properties. Analyses of variations in τ due to vegetation will be of interest in understanding how vegetation and soil moisture constrain each other.

Acknowledgments

K.A.M. is funded by a National Science Foundation Graduate Research Fellowship and a Ziff Environmental Fellowship from Harvard University's Center for the Environment. H.L. and W.W. are funded by the National Basic Research Program of China (2015CB953703) and the National Natural Science Foundation of China (91537210 and 41371328). The authors acknowledge funding from the MIT Greater China Fund for Innovation project "Global monitoring of the water cycle using new microwave space-borne instruments" and from the SMAP mission. All data used in this study are publicly available. The SMAP soil moisture data are available at https://nsidc.org/data/smap/smap-data.html. The soil texture data are available from N. Das on request (nndas@jpl.nasa.gov). The IGBP land cover data are available at http://lpdaac.usgs.gov. The GLDAS data are available at https://disc.sci.gsfc.nasa.gov/.

References

Bomblies, A., and E. A. B. Eltahir (2010), Assessment of the impact of climate shifts on malaria transmission in the sahel, *EcoHealth*, *6*(3), 426–437, doi:10.1007/s10393-010-0274-5.

Bonan, G. B., and L. M. Stillwell-Soller (1998), Soil water and the persistence of floods and droughts in the Mississippi River Basin, *Water Resour. Res.*, *34*(10), 2693–2701, doi:10.1029/98WR02073.

Botter, G., F. Peratoner, A. Porporato, I. Rodriguez-Iturbe, and A. Rinaldo (2007), Signatures of large-scale soil moisture dynamics on streamflow statistics across U.S. climate regimes, *Water Resour. Res.*, *43*, W11413, doi:10.1029/2007WR006162.

Brutsaert, W. (1982), *Evaporation Into the Atmosphere*, Springer, Netherlands.

Brutsaert, W. (2014), Daily evaporation from drying soil: Universal parameterization with similarity, *Water Resour. Res.*, *50*, 3206–3215, doi:10.1002/2013WR014872.

Champagne, C., T. Rowlandson, A. Berg, T. Burns, J. L'Heureux, E. Tetlock, J. R. Adams, H. McNairn, B. Toth, and D. Itenfisu (2016), Satellite surface soil moisture from SMOS and Aquarius: Assessment for applications in agricultural landscapes, *Int. J. Appl. Earth Obs. Geoinf.*, *45*, 143–154, doi:10.1016/j.jag.2015.09.004.

Chan, S. K., et al. (2016), Assessment of the SMAP passive soil moisture product, *IEEE Trans. Geosci. Remote Sens.*, *54*(8), 4994–5007, doi:10.1109/TGRS.2016.2561938.

Dardanelli, J. L., J. T. Ritchie, M. Calmon, J. M. Andriani, and D. J. Collino (2004), An empirical model for root water uptake, *Field Crops Res.*, *87*(1), 59–71, doi:10.1016/j.fcr.2003.09.008.

Das, N. (2013), SMAP ancillary data report: Soil attributes, *Tech. Rep. SMAP Sci. Doc. No. 044*, Jet Propulsion Lab., California Inst. of Technol., Pasadena, Calif.

Delworth, T. L., and S. Manabe (1988), The influence of potential evaporation on the variabilities of simulated soil wetness and climate, *J. Clim.*, *1*(5), 523–547, doi:10.1175/1520-0442(1988)001<0523:TIOPEO>2.0.CO;2.

D'Odorico, P., F. Laio, A. Porporato, and I. Rodriguez-Iturbe (2003), Hydrologic controls on soil carbon and nitrogen cycles. II. A case study, *Adv. Water Resour.*, *26*(1), 59–70, doi:10.1016/S0309-1708(02)00095-7.

Entekhabi, D., I. Rodriguez-Iturbe, and F. Castelli (1996), Mutual interaction of soil moisture state and atmospheric processes, *J. Hydrol.*, *184*(1–2), 3–17.

Entekhabi, D., et al. (2010), The Soil Moisture Active Passive (SMAP) mission, *Proc. IEEE*, *98*(5), 704–716, doi:10.1109/JPROC.2010.2043918.

Fecan, F., B. Marticorena, and G. Bergametti (1999), Parametrization of the increase of the aeolian erosion threshold wind friction velocity due to soil moisture for arid and semi-arid areas, *Ann. Geophys.*, *17*(1), 149–157, doi:10.1007/s00585-999-0149-7.

Ford, T. W., E. Harris, and S. M. Quiring (2014), Estimating root zone soil moisture using near-surface observations from SMOS, *Hydrol. Earth Syst. Sci.*, *18*(1), 139–154, doi:10.5194/hess-18-139-2014.

Friedl, M. A., D. Sulla-Menashe, B. Tan, A. Schneider, N. Ramankutty, A. Sibley, and X. Huang (2010), MODIS Collection 5 global land cover: Algorithm refinements and characterization of new datasets, *Remote Sens. Environ.*, *114*(1), 168–182, doi:10.1016/j.rse.2009.08.016.

Ghannam, K., T. Nakai, A. Paschalis, C. A. Oishi, A. Kotani, Y. Igarashi, T. Kumagai, and G. G. Katul (2016), Persistence and memory timescales in root-zone soil moisture dynamics, *Water Resour. Res.*, *52*, 1427–1445, doi:10.1002/2015WR017983.

Jacquemin, B., and J. Noilhan (1990), Sensitivity study and validation of a land surface parameterization using the HAPEX-MOBILHY data set, *Boundary Layer Meteorol.*, *52*(1–2), 93–134, doi:10.1007/BF00123180.

Katul, G. G., A. Porporato, E. Daly, A. C. Oishi, H.-S. Kim, P. C. Stoy, J.-Y. Juang, and M. B. Siqueira (2007), On the spectrum of soil moisture from hourly to interannual scales, *Water Resour. Res.*, *43*, W05428, doi:10.1029/2006WR005356.

Kerr, Y. H., et al. (2010), The SMOS mission: New tool for monitoring key elements of the global water cycle, *Proc. IEEE*, *98*(5), 666–687, doi:10.1109/JPROC.2010.2043032.

Konings, A. G., and P. Gentine (2016), Global variations in ecosystem-scale isohydricity, *Global Change Biol.*, *23*, 891–905, doi:10.1111/gcb.13389.

Koster, R. D., and M. J. Suarez (2001), Soil moisture memory in climate models, *J. Hydrometeorol.*, *2*(6), 558–570, doi:10.1175/1525-7541(2001)002<0558:SMMICM>2.0.CO;2.

Koster, R. D., and M. J. Suarez (2003), Impact of land surface initialization on seasonal precipitation and temperature prediction, *J. Hydrometeorol.*, *4*(2), 408–423.

Kurc, S. A., and E. E. Small (2004), Dynamics of evapotranspiration in semiarid grassland and shrubland ecosystems during the summer monsoon season, central New Mexico, *Water Resour. Res.*, *40*, W09305, doi:10.1029/2004WR003068.

Laio, F., A. Porporato, L. Ridolfi, and I. Rodriguez-Iturbe (2001a), Plants in water-controlled ecosystems: Active role in hydrologic processes and response to water stress: II. Probabilistic soil moisture dynamics, *Adv. Water Resour.*, *24*(7), 707–723.

Laio, F., A. Porporato, C. P. Fernandez-Illescas, and I. Rodriguez-Iturbe (2001b), Plants in water-controlled ecosystems: Active role in hydrologic processes and response to water stress: IV. Discussion of real cases, *Adv. Water Resour.*, *24*(7), 745–762, doi:10.1016/S0309-1708(01)00007-0.

Lorenz, R., E. B. Jaeger, and S. I. Seneviratne (2010), Persistence of heat waves and its link to soil moisture memory, *Geophys. Res. Lett.*, *37*, L09703, doi:10.1029/2010GL042764.

Mahfouf, J. F., C. Ciret, A. Ducharne, P. Irannejad, J. Noilhan, Y. Shao, P. Thornton, Y. Xue, and Z. L. Yang (1996), Analysis of transpiration results from the RICE and PILPS workshop, *Global Planet. Change*, *13*(1–4), 73–88, doi:10.1016/0921-8181(95)00039-9.

Manabe, S. (1969), Climate and the ocean circulation, *Mon. Weather Rev.*, *97*(11), 739–774, doi:10.1175/1520-0493(1969)097<0739:CATOC>2.3.CO;2.

Manzoni, S., J. P. Schimel, and A. Porporato (2012), Responses of soil microbial communities to water stress: Results from a meta-analysis, *Ecology*, *93*(4), 930–938, doi:10.1890/11-0026.1.

McColl, K., S. Alemohammad, R. Akbar, A. Konings, S. Yueh, and D. Entekhabi (2017), The global distribution and dynamics of surface soil moisture, *Nat. Geosci.*, *10*(2), 100–104.

O'Neill, P., S. Chan, E. Njoku, T. Jackson, and R. Bindlish (2016), SMAP L3 radiometer global daily 36 km EASE-grid soil moisture, version 2, *Tech. Rep.*, NASA Natl. Snow and Ice Data Cent. Distrib. Act. Arch. Cent., Boulder, Colo.

Orth, R., and S. I. Seneviratne (2012), Analysis of soil moisture memory from observations in Europe, *J. Geophys. Res.*, *117*, D15115, doi:10.1029/2011JD017366.

Pan, M., X. Cai, N. W. Chaney, D. Entekhabi, and E. F. Wood (2016), An initial assessment of SMAP soil moisture retrievals using high-resolution model simulations and in situ observations, *Geophys. Res. Lett.*, *43*, 9662–9668, doi:10.1002/2016GL069964.

Porporato, A., F. Laio, L. Ridolfi, and I. Rodriguez-Iturbe (2001), Plants in water-controlled ecosystems: Active role in hydrologic processes and response to water stress: III. Vegetation water stress, *Adv. Water Resour.*, *24*(7), 725–744, doi:10.1016/S0309-1708(01)00006-9.

Rodell, M., and H. Beaudoing (2007), GLDAS Noah land surface model l4 monthly 0.25 × 0.25 degree v001, *Tech. Rep.*, Goddard Earth Sci. Data and Inf. Serv. Cent. (GES DISC), Greenbelt, Md., doi:10.5067/7NP2052IA62C.

Rodriguez-Iturbe, I., A. Porporato, L. Ridolfi, V. Isham, and D. R. Coxi (1999a), Probabilistic modelling of water balance at a point: The role of climate, soil and vegetation, *Proc. R. Soc. A*, *455*(1990), 3789–3805, doi:10.1098/rspa.1999.0477.

Rodriguez-Iturbe, I., P. D'Odorico, A. Porporato, and L. Ridolfi (1999b), Tree-grass coexistence in Savannas: The role of spatial dynamics and climate fluctuations, *Geophys. Res. Lett.*, *26*(2), 247–250, doi:10.1029/1998GL900296.

Rondinelli, W. J., B. K. Hornbuckle, J. C. Patton, M. H. Cosh, V. A. Walker, B. D. Carr, and S. D. Logsdon (2015), Different rates of soil drying after rainfall are observed by the SMOS satellite and the South Fork in situ soil moisture network, *J. Hydrometeorol.*, *16*(2), 889–903, doi:10.1175/JHM-D-14-0137.1.

Rosenzweig, C., F. N. Tubiello, R. Goldberg, E. Mills, and J. Bloomfield (2002), Increased crop damage in the US from excess precipitation under climate change, *Global Environ. Change*, *12*(3), 197–202, doi:10.1016/S0959-3780(02)00008-0.

Saleem, J. A., and G. D. Salvucci (2002), Comparison of soil wetness indices for inducing functional similarity of hydrologic response across sites in Illinois, *J. Hydrometeorol.*, *3*(1), 80–91, doi:10.1175/1525-7541(2002)003<0080:COSWIF>2.0.CO;2.

Salvucci, G. D. (2001), Estimating the moisture dependence of root zone water loss using conditionally averaged precipitation, *Water Resour. Res.*, *37*(5), 1357–1365, doi:10.1029/2000WR900336.

Sellers, P. J., et al. (1997), Modeling the exchanges of energy, water, and carbon between continents and the atmosphere, *Science*, *275*(5299), 502–509, doi:10.1126/science.275.5299.502.

Seneviratne, S. I., et al. (2006), Soil moisture memory in AGCM simulations: Analysis of Global Land Atmosphere Coupling Experiment (GLACE) data, *J. Hydrometeorol.*, *7*(5), 1090–1112, doi:10.1175/JHM533.1.

Shellito, P. J., et al. (2016), SMAP soil moisture drying more rapid than observed in situ following rainfall events, *Geophys. Res. Lett.*, *43*, 8068–8075, doi:10.1002/2016GL069946.

Teuling, A. J., S. I. Seneviratne, C. Williams, and P. A. Troch (2006), Observed timescales of evapotranspiration response to soil moisture, *Geophys. Res. Lett.*, *33*, L23403, doi:10.1029/2006GL028178.

Teuling, A. J., R. Uijlenhoet, R. Hurkmans, O. Merlin, R. Panciera, J. P. Walker, and P. A. Troch (2007), Dry-end surface soil moisture variability during NAFE'06, *Geophys. Res. Lett.*, *34*, L17402, doi:10.1029/2007GL031001.

Tuttle, S. E., and G. D. Salvucci (2014), A new approach for validating satellite estimates of soil moisture using large-scale precipitation: Comparing AMSR-E products, *Remote Sens. Environ.*, *142*, 207–222, doi:10.1016/j.rse.2013.12.002.

Williams, C. A., and J. D. Albertson (2004), Soil moisture controls on canopy-scale water and carbon fluxes in an African savanna, *Water Resour. Res.*, *40*, W09302, doi:10.1029/2004WR003208.